nature chemical biology

ARTICLE

PUBLISHED ONLINE: 19 JANUARY 2014 | DOI: 10.1038/NCHEMBIO.1435

Integrated RAS signaling defined by parallel NMR detection of effectors and regulators

Matthew J Smith[1] & Mitsuhiko Ikura[1,2]*

The RAS GTPase directs cell proliferation and survival by selectively relaying signals amid a dynamic network of regulatory enzymes and protein interactions. Oncogenic mutation of RAS alters cell growth by deleteriously controlling output to RAS-binding effectors. Mechanisms underlying multieffector interactions for both wild-type and oncogenic RAS are poorly understood owing to challenges in quantifying outputs to multiple pathways in parallel. Using highly selective NMR probes for wild-type and oncogenic (G12V) RAS, we develop a systematic approach that quantitatively measures RAS output in composite mixtures of GEF, GAP and effector RAS-binding domains (RBDs). We derive effector signaling hierarchies and establish how oscillating concentrations generate effector 'switching'. The G12V mutation highly perturbs this system, specifically altering interactions with RAL GTPase-specific GEFs and RAF kinases. We further reveal that RAS–RBD complexes show extensive feedback to full-length regulatory proteins. Our approach quantifies output from signaling hubs, here providing an integrated view of the RAS network.

Cellular signaling networks are ordered by specific protein-ligand interactions that relay signals through distinct pathways. Generally, key signals are not transmitted through a single pathway by a single binding partner but rather through multiple proteins containing related domain modules that compete for inducible binding sites. Competition for ligands is influenced by the biophysical properties of individual complexes as well as spatiotemporal dynamics, gene expression and other factors. Current analyses of ever-expanding signaling transduction networks, however, lack systems-level quantification of output through multiple pathways, as experimental approaches able to precisely measure signals within an integrative framework are not available.

The RAS GTPase is a central, well-studied signaling hub highly implicated in human disease and a paradigm for current limitations in assaying complex signaling outputs. RAS proteins undergo conformational exchange between an active, GTP-bound state and an inactive, GDP-bound state to direct cell proliferation, differentiation and survival[1]. Inactivation via GTP hydrolysis is augmented by GTPase-activating proteins (GAPs), whereas a GDP-to-GTP exchange catalyzed by guanine nucleotide exchange factors (GEFs) promotes association with numerous downstream effector proteins[2]. Effectors bind specifically to RAS-GTP via RAS association (RA) domains or RAS binding domains (RBDs) that show wide-ranging affinities and thermodynamic characteristics[3–5]. There have been numerous studies on the structure and function of RAS and its associated proteins, and structural data (summarized in **Supplementary Table 1**) have explained how GAP proteins inactivate RAS[6] and the complex autoinhibitory mechanisms regulating RAS activation by the SOS1 GEF[7,8]. Data further illustrate how effector RBDs, though lacking extensive sequence conservation, share a common ubiquitin superfold structure (ββαββαβ) and conserved mode of RAS recognition (intermolecular, anti-parallel β-sheet consisting of β2 and β3 of RAS and β1, β2 and α1 of the RBD)[9–12].

It is thus clear that RAS signaling comprises a coordinated competition between effectors and regulatory proteins for a single nucleotide-binding site. Despite this, current models of the RAS network (as classically presented in **Fig. 1a**) are assembled using only isolated, one-to-one biochemical reactions and structural data. The resultant presumption, that GTPase networks function sequentially, provides a limited understanding of network dynamics as it disregards that both normal development and RAS-induced tumorigenesis depend on multiple downstream effectors that are typically expressed and localized together[2,13–16]. Furthermore, effector interactions compete directly with GAPs for RAS-GTP, and binding of the c-RAF1 RBD is known to sequester activated RAS from GAP-mediated hydrolysis[17–19]. Thus, new approaches that preserve a direct competition between effectors and regulatory proteins are required to elucidate and quantify signals from both wild-type and oncogenic RAS.

We now demonstrate properties of the integrated RAS network by parallel and quantitative analyses of complex RAS signaling modules. We have developed a systematic NMR approach that places RBDs in direct competition to reveal effector signaling hierarchies in a quantitative fashion. Markedly, oncogenic RAS^{G12V} exhibited a distinct effector binding profile that includes reduced interaction with RAFs and enhanced binding to RAL GTPase-specific GEFs (RALGEFs). Together with biophysical and cell-based data, we rationalize how modulating effector concentration influences cell signaling within an integrated network and how changes in affinity triggered by disease mutations affect the system. We further advance real-time detection of the RAS GTPase reaction[20] to establish that negative feedback from RAS-effector interactions controls output from the full-length regulatory proteins p120GAP and SOS1. This direct experimental approach can precisely quantify complex reactions in signaling modules and should be widely applicable to measure output from other key signaling hubs.

RESULTS

Effector binding hierarchies by direct competition

We hypothesized that NMR could evaluate interactions between RAS and multiple effectors in parallel, providing a precise, quantitative and integrated assessment of downstream output. To generate a pool of effector binding domains, we aligned amino acid sequences from 54 established or predicted RBD and RA domains (hereafter referred to collectively as RBDs) and chose ten from unique protein families that were expressed and purified to homogeneity (**Fig. 1b** and **Supplementary Results**, **Supplementary Fig. 1**).

[1]Campbell Family Cancer Research Institute, Ontario Cancer Institute, University Health Network, Toronto, Ontario, Canada. [2]Department of Medical Biophysics, University of Toronto, Toronto, Ontario, Canada. *e-mail: mikura@uhnresearch.ca

Alias names, related family members, downstream targets and proposed biological functions for these ten effector proteins are catalogued in **Supplementary Table 2**. We equilibrated individual RBDs and [^{15}N]RAS loaded with a nonhydrolyzable GTP-analog (GMPPNP) to examine their interaction with RAS. Binding of each domain to wild-type RAS and the oncogenic mutant G12V was confirmed by induction of multiple chemical shift perturbations in HSQC spectra (**Supplementary Fig. 2**). Association was saturated at 2:1 molar ratios of RBD to RAS. GRB10 showed no detectable interaction and henceforth serves as a control. We then used this panel of RBDs as a tool to study output from normal and mutant RAS.

One-to-one biochemical data have offered valuable insight to individual RAS-RBD complexes (summarized in **Supplementary Table 3** and **Supplementary Fig. 3**) but fail to predict how RAS selects between multiple effectors. Instead, we used NMR to place RBD domains in direct competition. Single domain interactions with [^{15}N]RAS-GMPPNP induce unique chemical shift profiles (**Fig. 1c**), making it possible to combine effectors and allow them to compete for RAS. To measure selectivity, two effector RBDs were equilibrated simultaneously with RAS-GMPPNP. Peak intensity measurements at chemical shifts characteristic of individual domain interactions establish precisely and quantitatively how RAS complexes with each RBD. Data are presented for the BRAF-ARAF and ARAF-RGL1 competitions in **Figure 1d**. BRAF strongly outcompeted ARAF, and we detected only BRAF-bound RAS chemical shifts upon co-equilibration with these RBDs. Conversely, addition of ARAF and RGL1 induced RAS chemical shifts specific to each domain, and quantification of peak intensities determined a ratio of 62% ARAF to 38% RGL1 (± 1.5% s.d.). This analysis was performed for all pairwise combinations of RBDs (**Supplementary Table 4a**). We compiled these data to determine a hierarchy of integrated RAS effector interactions that begins with the tight-binding BRAF RBD and ends with RGS14 (**Fig. 2a**). As this assay placed effector domains in direct competition, it establishes selectivity without the necessary inferences derived from one-to-one biochemical data.

It is unlikely that proteins at the bottom of the hierarchy could compete for active RAS in cells. Enhanced proximity to RAS or increased gene expression may augment the concentration of these effectors to better compete for RAS-GTP. To explore this, we considered that effector RBDs in the central region of the hierarchy should demonstrate 'switching' upon slight variations in concentration, whereas those further apart would be less sensitive to concentration changes. We thus measured binding of two RBDs to RAS-GMPPNP in parallel at four molar ratios. ARAF and RGL1 reside in close proximity in the hierarchy, and fluctuations in their concentration redistributed RAS between ARAF- and RGL1-bound states (**Fig. 2b**). In contrast, even a twofold excess of RALGDS was unable to sequester RAS from ARAF. These data reflect the importance of oscillating effector concentrations and make evident that slight changes in the concentration of domains with similar binding properties can substantially perturb a signaling system.

Quantifying signals within an integrated network represents a major challenge for modern biology. As our assay provides measureable data that reflects downstream output from RAS, we postulated that our results could be extrapolated to estimate the capacity for each domain to compete for RAS at any given concentration. Having directly measured RAS binding to shifting concentrations of RGL1 and ARAF, we found these data fit nicely to nonlinear models with an exponential distribution (**Fig. 2c**). These curves establish relative binding to RAS at any given ratio of ARAF to RGL1. Furthermore, the complete hierarchy was determined by challenging RAS with equimolar concentrations of two RBDs (1:1), and by adding two constraints (requirements that

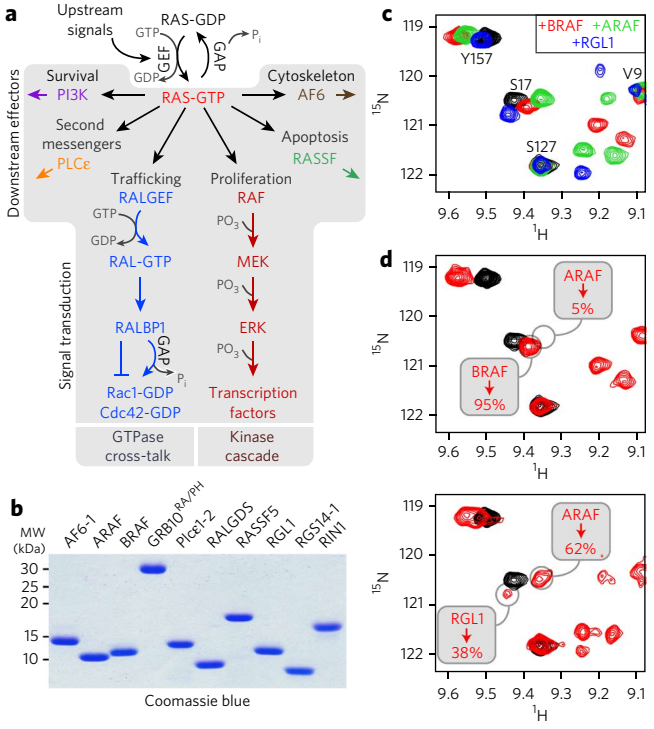

Figure 1 | Quantification of effector signaling by parallel detection of multiple RBD domains binding to [^{15}N]RAS-GTP. (**a**) RAS signaling revolves around the GTPase cycle, whereby RAS is activated when GEFs catalyze a GDP-to-GTP exchange. Intrinsic hydrolysis of GTP is slow, and RAS inactivation requires the activity of GAPs. RAS-GTP binds numerous effectors, which relay signals through diverse intracellular pathways. Downstream signals through two effector pathways are extended here: the kinase cascade induced by RAF (red) and the cross-talk to RAL and RHO family GTPases following RAS binding to RALGEFs (blue). (**b**) Ten RBDs were expressed and purified to homogeneity from *Escherichia coli*. Domain boundaries were established through alignments and secondary structure predictions. Uncut gels are in **Supplementary Figure 8a**. (**c**) Individual RBDs induce unique chemical shift perturbations in RAS ^{1}H-^{15}N HSQC spectra. All of the individual domains were mixed in a twofold molar excess of [^{15}N]RAS-GMPPNP; shown here are BRAF (red), ARAF (green) and RGL1 (blue). (**d**) Direct competition between RBDs as measured by simultaneous mixing. Top, addition of BRAF and ARAF; HSQC overlay shows predominantly BRAF-bound chemical shifts. Bottom, addition of ARAF and RGL1 generates chemical shifts characteristic to both domains. Intensity measurements provide a ratio (inset; as percentage).

0% or 100% of any RBD bind 0% or 100% of RAS, respectively), we could generate models that offer predictions of RAS binding that correlate extremely well with direct NMR measurements (**Fig. 2d**). This analysis was extended to the complete RAS effector hierarchy by fitting averaged data to exponential models, providing estimates of output to RBDs in complex mixtures (**Fig. 2e** and **Supplementary Fig. 4**). As an example, we can project that 50% of RAS signals through RALGDS if it is present at 73% in a mixed RBD population. As activated RAS in cells is likely to encounter a diverse set of effector proteins, extrapolations of RAS binding based on directly measured, parallel RBD interactions offers powerful quantification of systems-level output within an integrated network.

Differential effector usage by RAS^{G12V}

Approaches that provide quantitative signaling data would greatly benefit efforts at characterizing disease mutations. For RAS, establishing whether oncogenic mutants alter signaling through

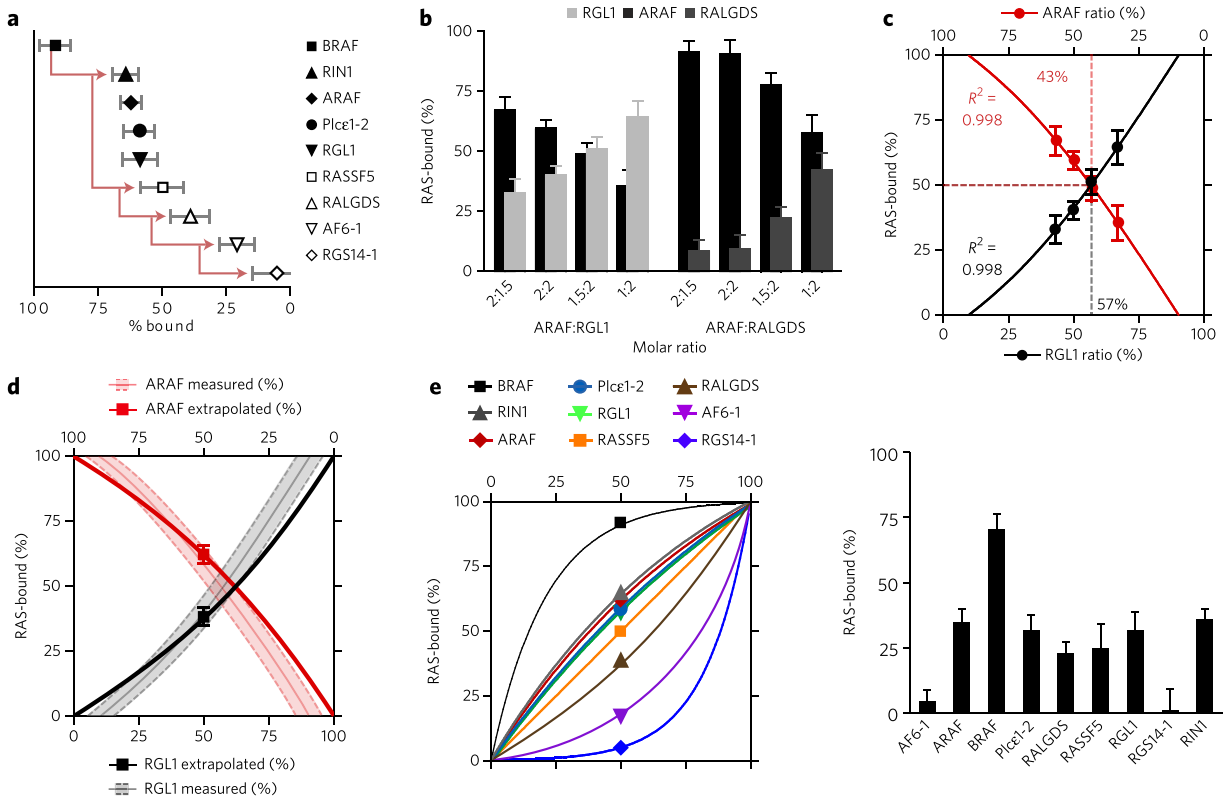

Figure 2 | Establishing an RBD binding hierarchy. (**a**) Plot of average percentage bound for each RBD following pairwise competition reveals RAS selectivity. Error bars are derived from ratio differences between individual sets of measured resonance intensities (n = 5). Apparent steps in the hierarchy are indicated by arrows (red). (**b**) Effector 'switching' by fluctuating RBD concentrations. Left, RAS binding interconverts with shifting ratios of ARAF (black) and RGL1 (light gray). Right, a twofold excess of RALGDS (dark gray) cannot appropriate RAS binding from ARAF (black). Plots display average percentage bound, and error bars are from differences between resonance intensities (n = 5). (**c**) Extrapolating RGL1 and ARAF competition across concentrations. Curves were generated by nonlinear regression for RGL1 (black) and ARAF (red) binding to RAS. Important benchmarks can be extracted, as indicated for 50% association with RAS. (**d**) Hierarchical analysis indicated that 62% RAS is bound to ARAF and 38% is bound to RGL1. Curves were extrapolated for ARAF (red) and RGL1 (black) by adding two constraints: RBD at 0% or 100% of the population binds 0% or 100% of RAS, respectively. Curves correlate well with those derived from direct NMR measurements (dashed lines, from **c**). (**e**) Hierarchical data for all of the RBDs extrapolated to estimate RAS output. Averaged binding (plus constraints, as in **d**) generates curves reporting RAS-bound for each RBD in a mixed population. Right, benchmark values can be extracted; here they report the percentage of RAS bound with each RBD at 25%. Error bars represent 90% confidence intervals derived from the standard error of fit for each curve.

specific downstream pathways could provide important targets for drug discovery. Oncogenic mutations are typically located around the RAS switch regions that mediate both nucleotide and effector binding, yet surprisingly few data exist describing oncogenic RAS binding to RBDs. We thus repeated the complete competition assay using RAS^{G12V} (**Fig. 3a** and **Supplementary Table 4b**). Although BRAF again resides at the top position, several intriguing distinctions are apparent (**Fig. 3b**). ARAF exhibited greater binding to wild-type RAS (18%), whereas RGL1 and RALGDS (both GEFs for RAL GTPases) were higher in the RAS^{G12V} hierarchy (13% and 16%, respectively). This implied a possible discrepancy in signaling output to these effectors.

To validate this, we first used NMR to analyze binding of RAS^{G12V} to ARAF and RGL1 using the relative RBD concentrations previously probed against wild-type RAS. Remarkably, we could directly observe that RGL1 and ARAF no longer demonstrate switching when competing for RAS^{G12V}, as RGL1 sequesters mutant RAS from ARAF over the entire concentration range (**Fig. 3c**,**d**). A similar experiment with ARAF and RALGDS established that RAS^{G12V} binding interconverts between these RBDs, in direct contrast to wild-type RAS (**Supplementary Fig. 5a**,**b**). We extrapolated from these data the full capacity for RGL1 to compete with ARAF, verifying that RGL1 must be present in higher quantities to bind wild-type RAS compared with RAS^{G12V} (**Supplementary Fig. 5c**,**d**). Finally, following regression analysis of the complete RAS^{G12V}-RBD hierarchy (as done for wild-type RAS; **Fig. 2e**), benchmark comparisons indicated that ARAF and BRAF are better substrates for the wild type, whereas RGL1 and RALGDS are favored by RAS^{G12V} (**Supplementary Fig. 5e–g**).

We postulated that changes in affinity to these RBDs resulting from the G12V mutation could affect a substantial reordering of the hierarchy, analogous to concentration-dependent switching. We therefore chose to further investigate wild-type RAS and RAS^{G12V} interactions with ARAF and RGL1 using isothermal titration calorimetry (ITC). RBDs were injected into wild-type RAS or RAS^{G12V} loaded with GMPPNP (**Fig. 3e** and **Supplementary Fig. 6a**). In agreement with our determined hierarchies, ARAF had a higher affinity for wild-type RAS (0.89 ± 0.06 μM) than RAS^{G12V} (1.80 ± 0.09 μM), whereas RGL1 showed higher affinity for RAS^{G12V} (1.19 ± 0.01 μM) compared to wild-type (1.78 ± 0.13 μM). ARAF thus has a twofold higher affinity for wild-type RAS than does RGL1, but its affinity to G12V is 35% weaker. Interestingly, both RBDs bound with distinct stoichiometries to wild-type (n = 0.6) and RAS^{G12V} (n = 0.3) that correlate directly with ^{31}P-NMR data describing differential equilibria of two conformations (state 1 and 2) of their effector-binding loops[21–23]. We verified our data by performing the reverse ITC experiment, which corroborated that RGL1 has a higher affinity for RAS^{G12V} and that ARAF has a higher affinity

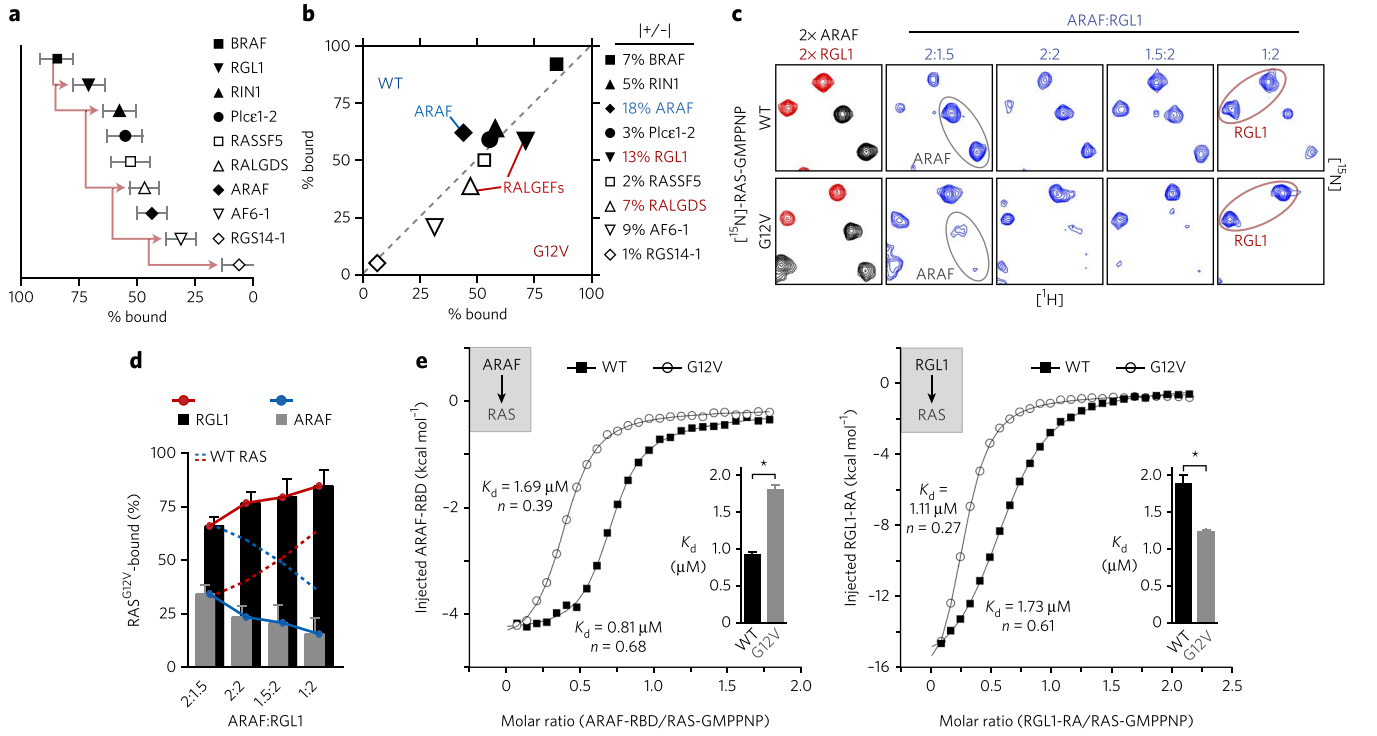

Figure 3 | RAS^{G12V} demonstrates distinct effector usage. (**a**) Hierarchy plot of percentage RAS^{G12V} bound following pairwise competition reveals RBD selectivity. Hierarchical phases indicated by arrows (red). Error bars derived from ratio differences between individual sets of measured resonance intensities (n = 5). (**b**) Direct comparison of effector binding to wild-type RAS (left, blue) versus G12V (bottom, red). Domains from RALGEFs and ARAF exhibit particularly large shifts. The absolute change in binding (%) is adjacent to each domain. (**c**) HSQC spectra of [^{15}N]RAS reveal competitive binding between ARAF and RGL1. Left, RAS cross-peaks generated by RAS binding independently to RGL1 (red) or ARAF (black) are well dispersed in this region. Top, wild-type RAS mixed simultaneously with 2:1.2, 2:2, 1.5:2 or 1:2 molar ratios of ARAF and RGL1 (blue). Bottom, identical series of competition assays performed with RAS^{G12V}. (**d**) Using the same RGL1 and ARAF concentration range over which wild-type (WT) RAS interconverts (dashed lines), RAS^{G12V} no longer demonstrates switching, and RGL1 (black) sequesters the majority of RAS^{G12V} from ARAF (gray). (**e**) ITC experiments confirm preferential binding of ARAF and RGL1 to wild-type RAS and RAS^{G12V}, respectively. Left, ARAF-RBD injected into wild-type or RAS^{G12V}-GMPPNP. Resultant dissociation constants (K_d) and stoichiometry (n) are denoted next to curves. Right, RGL1-RBD injected into wild-type RAS or RAS^{G12V}-GMPPNP shows an inverse binding preference. Inset, bar graphs of dissociation constants demonstrate reversing affinities (data represent mean values ± s.d.). *P < 0.01; significance determined by a two-tailed, unpaired t-test.

for the RAS (**Supplementary Fig. 6b**,**c**). These data support our hypothesis that mutation-driven changes affecting the binding properties of individual complexes in a hierarchy can extensively perturb a signaling system. They also indicate that oncogenic mutations not only affect RAS GTPase cycling but also can differentially influence effector binding.

Divergent effector signaling from RAS^{G12V} in cells

Quantifying output to multiple pathways *in vivo* is extremely challenging, driving the need for *in vitro* experimental approaches that directly measure integrated biochemical signals. Nevertheless, we sought to directly compare RAS signals relayed to RALGEFs and RAFs in cells, as a reversed preference could have major consequences for oncogenic RAS signaling. Indeed, recent data have delineated the importance of RALGEFs to tumorigenesis[24–26]. To study the RAS network in cells, one must consider several RAS isoforms, effector proteins with numerous family members (i.e. c-RAF-1, BRAF and ARAF), and that multiple effectors are co-expressed. Moreover, the RAS activation level in any given cell is reflected in the regulatory activity of several GEFs and GAPs, and all of the network components may present distinct spatiotemporal dynamics. This analysis is further complicated in that RAS^{G12V} and wild-type RAS have very distinct nucleotide exchange and hydrolysis properties[20], necessitating an approach that measures output from comparable activation states. To achieve this, we expressed wild-type RAS or RAS^{G12V} together with the catalytic domain of SOS1 (SOS^{cat})[7] fused to a membrane-targeting CaaX sequence to drive constitutive nucleotide exchange. **Figure 4a** shows that wild-type RAS and RAS^{G12V} are uniformly activated in the presence of SOS^{cat}-CaaX. Further, after passage through a BRAF-RBD affinity column, both wild-type RAS and RAS^{G12V} are cleared from lysates when expressed together with SOS^{cat}-CaaX (**Supplementary Fig. 7a**). Thus, our approach provides an *in vivo* system in which we can differentiate effector outputs from wild-type RAS and RAS^{G12V} in analogous activation states.

To quantify RAS signaling through RALGEFs, we used the RALA-binding domain from RALBP1 to probe RALA-GTP[27], and we monitored levels of pERK to measure RAF output (**Fig. 1a**). In starved cells, we observed negligible amounts of pERK, but the RALA pathway was highly activated. Conversely, stimulation with EGF substantially induced pERK but only marginally augmented RALA-GTP (**Fig. 4b** and **Supplementary Fig. 7b**). This indicates that RALGEFs are proximal to RAS-GTP in the absence of EGF stimulation, but RAF kinases require upstream cues for their recruitment. Thus, although it is not possible to precisely regulate the concentration and localization of effectors *in vivo* to drive antagonism (as with our NMR assays), EGF stimulation generates a direct competition for RAS association between RALGEFs and recruited RAF kinases. We subsequently expressed SOS^{cat}-CaaX and either wild-type RAS or RAS^{G12V} in parallel and directly measured RALA-GTP and pERK in starved cells or after 5 min, 15 min or 45 min of EGF stimulation (**Fig. 4c**). This was repeated

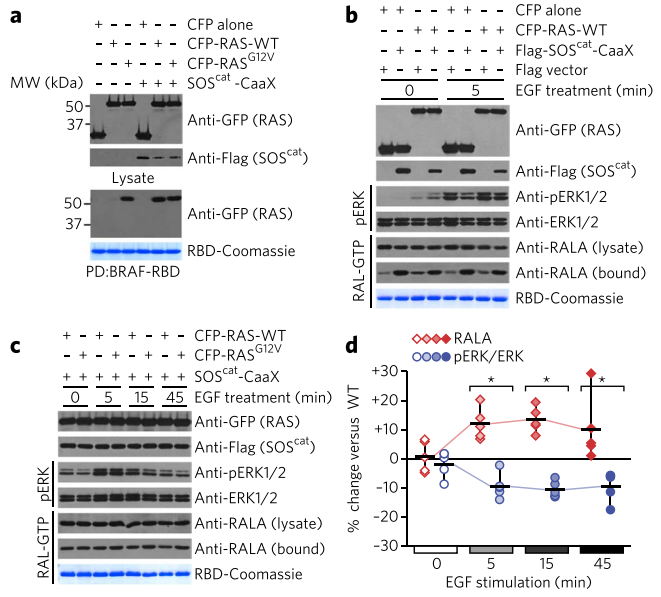

Figure 4 | Wild-type RAS and RAS^{G12V} show opposing activation of RALA and ERK. (**a**) Co-expression with SOS^{cat}-CaaX activates RAS. CFP-tagged, full-length wild-type (WT) RAS or RAS^{G12V} were expressed in HEK 293 cells. Top, loading of RAS (anti-GFP) and SOS^{cat}-CaaX (anti-Flag). Bottom, interaction with BRAF-RBD determined RAS-GTP levels. CFP alone or empty Flag vector were used as controls. PD, pulldown. (**b**) Measuring effector output downstream of RAS in the presence of SOS^{cat}-CaaX. Vector control or Flag-SOS^{cat}-CaaX were co-expressed with CFP alone or CFP-tagged wild-type RAS. Cells were starved (0 min) or stimulated with EGF (5 min). Shown are expression levels of RAS (anti-GFP), SOS^{cat}-CaaX (anti-Flag), ERK (anti-ERK1/2) and RALA (anti-RALA, lysate). Immunoblotting of pERK (anti-pERK1/2) quantified signals downstream of RAF, and interaction with the RALA binding domain (RALBP1) quantified signaling to RALGEFs (anti-RALA, bound). (**c**) Comparison of output from wild-type RAS and RAS^{G12V}. Shown are expression levels of RAS (anti-GFP), SOS^{cat}-CaaX (anti-Flag), ERK (anti-ERK1/2) and RALA (anti-RALA, lysate) in starved cells or following EGF stimulation (5 min, 15 min and 45 min). Immunoblotting of pERK (anti-pERK1/2) quantified RAF signals, and interaction with RALBP1 Coomassie blue) determined RALGEF signals (anti-RALA, bound). (**d**) Results from five independent experiments showing levels of RALA-GTP (red) and pERK (blue) induced by RAS^{G12V} compared to the wild type. Individual experiments were quantified by densitometry and normalized to obtain percentage change for starved cells (0 min) and after 5 min, 15 min or 45 min of EGF stimulation. Mean differences are denoted by solid line. *$P < 0.05$; significance determined by a two-tailed, paired *t*-test. Uncut gels are in **Supplementary Figure 8**.

five separate times, revealing that RAS^{G12V} activates significantly higher RALA-GTP levels than the wild type, whereas wild-type RAS induces significantly higher quantities of pERK (**Supplementary Fig. 7c,d**; $P < 0.05$). **Figure 4d** presents every data point from these experiments, contrasting RAS^{G12V} output with that of wild-type RAS. Although signaling to the RALA and ERK pathways is comparable in starved cells, RAS^{G12V} consistently generates ~10–15% more RALA-GTP and ~10% less pERK than wild-type RAS following EGF treatment. These data correlate well with hierarchical shifts detected by NMR and also highlight the RAL pathway as a specific therapeutic target in RAS^{G12V}-transformed cells.

Effector binding sequesters RAS-GTP from GAPs

In an integrated RAS network, we must consider how regulation via GAP and GEF proteins might interplay with effector binding. We thus sought to expand the utility of our NMR assay to examine the impact of regulatory enzymes. It has been proposed that the short lifetime of RAS–RBD complexes allows GAP access to RAS-GTP[28–30], providing strict temporal regulation. However, the RBD of c-RAF1 is known to inhibit GAP activity[17–19], and we considered whether this was specific or a more general property of RBDs. To test this, [^{15}N]RAS was loaded with GTP and incubated with the bacterially expressed catalytic region of p120GAP (GAP-334 (ref. 6)). Hydrolysis was measured[20] in the presence or absence of twofold molar excess of RBD (**Fig. 5a** and **Supplementary Fig. 9a**). At a ratio of 1:5,000, GAP-334 stimulates GTP hydrolysis sixfold (**Supplementary Table 5** contains details for all NMR-based GTPase assays). Sensitivity to GAP-334 was completely abolished in the presence of all effector domains but was maintained in the GRB10 control (**Fig. 5b**). Work on p120GAP has suggested that the full-length protein retains 20-fold more activity than the C-terminal fragment alone[31], and we therefore assessed whether full-length p120GAP might better compete with effectors. Lysates from cells expressing Tet-inducible, Flag-tagged p120GAP were monitored for GAP activity by NMR[20]. Lysate from Tet-induced cells increased hydrolysis rates fivefold over a corresponding quantity of control lysate, and the presence of RALGDS-RBD resulted in complete inhibition of full-length p120GAP-catalyzed hydrolysis (**Fig. 5c**). Similar results were obtained for all effectors (**Fig. 5d** and **Supplementary Fig. 9b**). These data provide evidence that neither associated domains in p120GAP nor additional factors in cell lysates (i.e. phosphorylation or accessory proteins) are able to increase GAP access to RAS in the presence of bound effector.

The binding constant for GAP to RAS-GTP is relatively low (17 μM)[32]. Thus, we investigated the effects of titrating increasing concentrations of GAP to examine its relationship with the effector hierarchy. Addition of GAP-334 at 1:100 or 1:10 molar ratios induced GTP hydrolysis in the presence of RIN1, which nonetheless retained a remarkable inhibitory property considering the high concentrations of GAP and the long time interval (**Fig. 5e**). The binding constant reported for RIN1-RBD to RAS-GTP is 0.9 μM (ref. 4). To extend our analysis, titrations of GAP-334 were performed in the presence of ARAF-RBD, which has a comparable affinity for RAS-GTP as RIN1 (0.7 μM)[33], and the weak-binding AF6-RBD (2.2 μM)[4]. Consistent with these data and our effector hierarchy, lower concentrations of GAP-334 activated RAS hydrolysis in the presence of AF6 compared with ARAF or RIN1 (**Fig. 5f**). Nevertheless, AF6 showed substantial inhibition of GAP-mediated hydrolysis at even a 1:100 ratio with GAP-334. Taken together, reconstitution of RAS downstream signaling for NMR has made evident that there is direct competition for RAS-GTP existing between effector and GAP proteins, that RBD-bound RAS is highly resistant to GAP over long time intervals (minutes) and that GAP itself should be fit in the hierarchy downstream of activated RAS.

Allosteric SOS1 activation is modulated by effectors

Activation of the SOS1 GEF requires RAS binding to an allosteric site in its REM domain. This site is occluded by an autoinhibitory module consisting of the HF and DH-PH domains in the full-length GEF[8,34]. The affinity of 'active' RAS-GTP for the allosteric site (4 μM) is higher than that of GDP-bound RAS (25 μM)[35], suggesting that RBDs may block positive feedback to full-length SOS1 by sequestering RAS-GTP. Indeed, a structural analysis of RAS residues involved in complex with RBDs, GAP-334 or the SOS^{cat} REM domain demonstrates their overlapping binding interface (**Fig. 6a**). To test whether RBDs inhibit SOS1, both wild-type and a hyperactive SOS1 mutant in which the allosteric site is exposed (mutations in the DH domain and PH-REM domain linker (DH/Link): E268A, M269A, D271A and R552G)[20] were expressed in HEK 293 cells. Cell extracts were added directly to [^{15}N]RAS and a tenfold molar excess of GTPγS in the presence or absence of a twofold excess BRAF-RBD. These assays established that wild-type SOS has a fourfold increased exchange

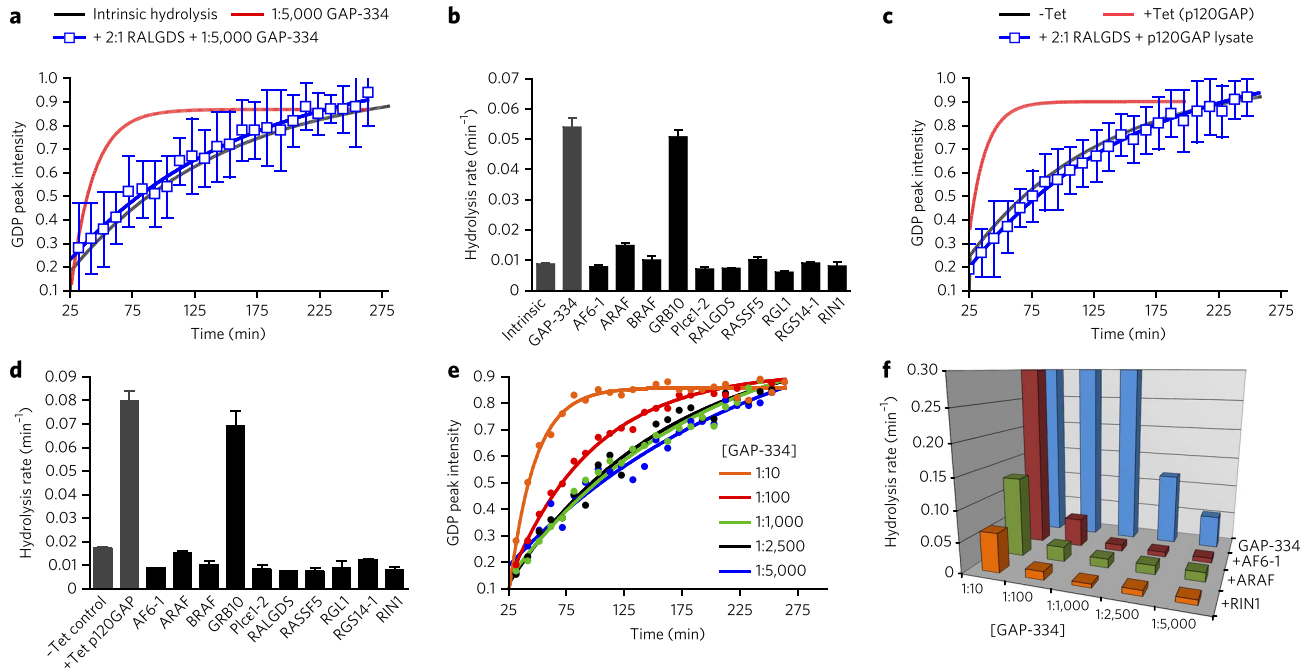

Figure 5 | RBD–RAS complexes inhibit GAP activity. (**a**) NMR-based GAP-334 assay performed in the presence of the RALGDS RBD. Typical hydrolysis rates induced by 1:5,000 GAP-334 revert to intrinsic rates when mixed with a twofold molar excess of RBD. (**b**) All RBDs show complete inhibition of GAP-334. Plot shows NMR-derived hydrolysis rates for 1:5,000 GAP-334 in the presence of a 2:1 molar excess of RBD. GRB10 served as a negative control. Error bars were derived from two or more replicates (data represent mean values ± s.d.). (**c**) Activity of full-length p120GAP is inhibited by RBDs. Tet-induced p120GAP stimulates RAS GTP hydrolysis, whereas control lysates show near-intrinsic rates. A twofold molar excess of RALGDS-RBD completely inhibits p120GAP activity. (**d**) All RBDs inhibited full-length p120GAP activity. GRB10 again served as a control (data represent mean values ± s.d.). (**e**) Increasing concentrations of GAP-334 compete with effector domains. GAP-334 was added in ratios up to 1:10 in the presence of 2:1 RIN1 RBD. GTP hydrolysis curves were measured by NMR. (**f**) Weak binding RBDs from the bottom of the hierarchy are displaced by GAP-334 at lower molar ratios. Greater amounts of GAP-334 are required to compete out ARAF (green) or RIN1 (orange) compared with AF6 (red). In the absence of RBD, addition of only 1:1,000 GAP-334 results in hydrolysis rates much faster than our time resolution (blue). Error bars in **a** and **c** show s.d.

rate over a vector control, with SOS-DH/Link showing a further fivefold increase. Both wild-type and hyperactive SOS1, however, were completely unable to stimulate exchange in the presence of BRAF-RBD (**Fig. 6b**). To further examine the direct competition between effector RBDs and the SOS1 allosteric site for RAS-GTP, we performed a titration with RALGDS. SOS1-mediated RAS exchange was completely inhibited at a 2:1 ratio with RALGDS, and increasing GEF activity was detected with decreasing RBD concentrations (**Fig. 6c**). These data demonstrate that full-length SOS1 is dependent on positive feedback from GTP-bound RAS and reveal that effector binding is antagonistic not only to GAPs but also to the allosteric mechanism controlling SOS1 activation.

DISCUSSION

Large-scale detection of protein interactions provides an ever-expanding network of associated signaling proteins. Systems biology approaches attempt to integrate diverse data sets to measure output through distinct pathways but greatly require direct experimental methods to detect and quantify integrated signal outputs. This is particularly true for GTPases and other key signaling hubs that have a vital role in organizing cellular responses. We have developed a systematic approach using NMR probes for RAS to measure the combined influence of GAPs, GEFs and effector RBDs. Our NMR methodology provides residue-specific observations of integrated RAS signaling modules, including real-time quantification of outputs through multiple pathways in parallel.

The human proteome encodes over 50 RBD-containing proteins (**Supplementary Fig. 1a**). Although RBD and RA domains lack extensive sequence homology, they share a common ubiquitin superfold structure and conserved mode of RAS recognition that makes effector activation a paradigm for the challenge in studying integrated signaling, as both transformation and normal development depend on multiple effector pathways. This is exemplified by the differential efficacy of effector-targeted therapeutics in cancer[36–38] and by observations of effector 'switching' as a developmental strategy[15]. Placing RBDs in direct competition and allowing their inherent thermodynamic and kinetic properties to govern RAS selectivity allowed us to establish an unambiguous hierarchy of RBD binding. The central region of this hierarchy revealed how oscillating RBD concentrations can 'switch' effector output. Furthermore, we could extrapolate the capacity for every RBD to bind RAS at any occupancy in a mixed population of competing domains. Ultimately, overlaying with expression profiles or spatiotemporal data should provide accurate estimates of RAS output directly dependent on effector availability.

Our data reveal a marked affinity reversal of oncogenic RAS^{G12V} for RGL1 and ARAF that extensively alters its effector binding hierarchy and proportionally transforms output *in vivo*. These results are highly relevant to the development of RAS pathway therapeutics, as effectors displaying increased prominence in mutant RAS hierarchies may prove important for mediating transformation and may also render cells expressing oncogenic RAS susceptible to targeting of these pathways. We postulate that major variations in the dynamics of the RAS switch I region, previously established for wild-type RAS and RAS^{G12V} by ^{31}P-NMR[21–23], are responsible for the observed discrepancy in effector binding. Indeed, our ITC data were markedly consistent with ^{31}P-NMR data and demonstrate how RAS state 1-2 exchange affects effector binding in solution. The switch I loop is likely to sample numerous low-populated structural conformations upon RAS state switching, which could

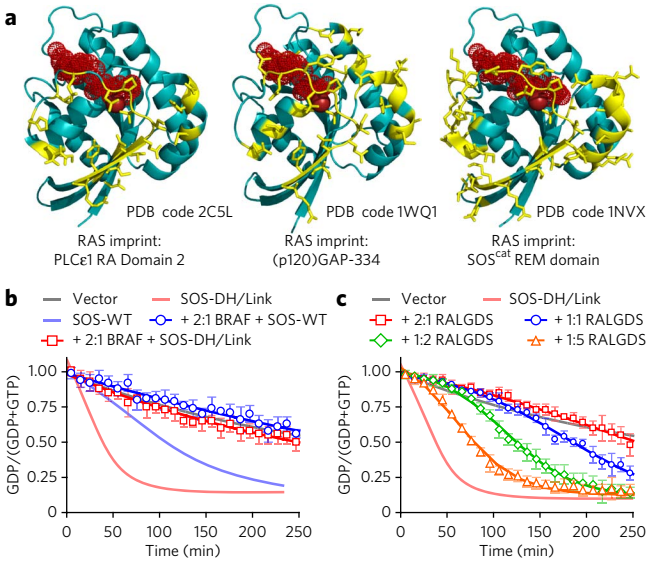

Figure 6 | RBDs inhibit full-length SOS1 by preventing its allosteric activation. (**a**) Structural analysis of RAS binding by RBD, GAP and the SOS1/REM domain allosteric site. Highlighted are RAS residues (yellow) within 3 Å of these associated proteins, in three individual crystal structures. Left, imprint from the PLCε1 RA-2 domain (Protein Data Bank (PDB) code 2C5L); middle, from GAP-334 (PDB code 1WQ1); right, from SOS^{cat} (PDB code 1NVX). Nucleotides are shown in red (dots), and Mg^{2+} is shown in dark red (sphere). RAS residues outside of the interface are in blue (ribbons). (**b**) Exchange activity of cell extracts containing full-length wild-type (WT) SOS1 or hyperactive SOS-DH/Link are completely inhibited by a 2:1 molar excess BRAF-RBD. Rates revert to those exhibited by a vector control. (**c**) As with GAPs, the capacity for RBDs to inhibit SOS1 results from a direct competition for RAS. Decreasing ratios of RALGDS-RBD were added to exchange reactions driven by lysates expressing hyperactive SOS-DH/Link. Rates of RAS exchange increase with reduced RBD concentrations. The rate is similar to a vector control at 2:1 RALGDS.

highly affect electrostatically driven effector interactions governed by the spacing of charged residues on the surface of RBDs[22,39–41]. Our biochemical data revealing enhanced binding of RAS^{G12V} to RALGEFs is also consistent with several recent observations recognizing the importance of this pathway to oncogenesis[24,25] and that RALGEFs are activated in RAS-driven pancreatic cancers without a corresponding increase in RAF signaling[26].

A fundamental yet underappreciated aspect of the GTPase field is the relationship between effector binding and regulatory GAPs and GEFs. Understanding this interplay is vital when considering signal output from the whole network. GAPs are presumed to function as 'negative regulators' that rapidly inactivate RAS-GTP in cells owing to the short lifetime of RAS–RBD complexes[28–30]. Our results, however, indicate that RBD-bound RAS is remarkably resistant to GAP activity over long time intervals. This strongly suggests that effectors 'trap' a fraction of active RAS in cells, whereas GAP proteins act upon free RAS-GTP (i.e. reducing noise in the system). Inactivation of effector-bound RAS is clearly required for proper spatiotemporal regulation and can be rationalized by a combination of ubiquitination[42], spatial sorting[43,44], phosphorylation[45] and negative feedback from downstream pathways[46,47].

Although previous work had implied antagonism between GAPs and effectors, we identify here a similar mechanism that highly modulates SOS1 GEF activity. Positive feedback from RAS-GTP to an allosteric site in the SOS1 REM domain has been characterized[48,49], and our data reveal that this feedback is regulated in a negative manner by competition with effector RBDs. These data highlight how an integrated mechanism contributes to the amplitude and duration of SOS1-mediated RAS exchange. Constitutively GTP-bound RAS oncogenic mutants would circumvent this negative feedback (not being permanently effector bound[50]), enhancing allosteric SOS1 activation.

In this paper, we have shown how NMR offers a powerful readout for studying integrated signaling. We identified a role for RAS effectors in negative feedback to regulatory proteins, ordered effector signaling downstream of RAS and revealed a new mechanism by which oncogenic RAS^{G12V} alters signals. Quantitative experimental approaches, such as that described here, allow reconstitution of integrated signaling modules and will prove important to future efforts at quantifying outputs to specific pathways. Indeed, our approach can now be applied to quantify signals downstream of phosphorylation sites (or other key binding motifs), observe antagonism between nucleic acid-binding proteins or study the influence of small-molecule modulators on network properties.

Received 3 June 2013; accepted 26 November 2013; published online 19 January 2014

METHODS

Methods and any associated references are available in the online version of the paper.

References

1. Vetter, I.R. & Wittinghofer, A. The guanine nucleotide-binding switch in three dimensions. *Science* **294**, 1299–1304 (2001).
2. Rodriguez-Viciana, P., Sabatier, C. & McCormick, F. Signaling specificity by Ras family GTPases is determined by the full spectrum of effectors they regulate. *Mol. Cell. Biol.* **24**, 4943–4954 (2004).
3. Rudolph, M.G. *et al.* Thermodynamics of Ras/effector and Cdc42/effector interactions probed by isothermal titration calorimetry. *J. Biol. Chem.* **276**, 23914–23921 (2001).
4. Wohlgemuth, S. *et al.* Recognizing and defining true Ras binding domains I: biochemical analysis. *J. Mol. Biol.* **348**, 741–758 (2005).
5. Kiel, C., Foglierini, M., Kuemmerer, N., Beltrao, P. & Serrano, L. A genome-wide Ras-effector interaction network. *J. Mol. Biol.* **370**, 1020–1032 (2007).
6. Scheffzek, K. *et al.* The Ras–RasGAP complex: structural basis for GTPase activation and its loss in oncogenic Ras mutants. *Science* **277**, 333–338 (1997).
7. Margarit, S.M. *et al.* Structural evidence for feedback activation by Ras. GTP of the Ras-specific nucleotide exchange factor SOS. *Cell* **112**, 685–695 (2003).
8. Gureasko, J. *et al.* Role of the histone domain in the autoinhibition and activation of the Ras activator Son of Sevenless. *Proc. Natl. Acad. Sci. USA* **107**, 3430–3435 (2010).
9. Nassar, N. *et al.* The 2.2 Å crystal structure of the Ras-binding domain of the serine/threonine kinase c-Raf1 in complex with Rap1A and a GTP analogue. *Nature* **375**, 554–560 (1995).
10. Huang, L., Hofer, F., Martin, G.S. & Kim, S.H. Structural basis for the interaction of Ras with RalGDS. *Nat. Struct. Biol.* **5**, 422–426 (1998).
11. Pacold, M.E. *et al.* Crystal structure and functional analysis of Ras binding to its effector phosphoinositide 3-kinase γ. *Cell* **103**, 931–943 (2000).
12. Kiel, C., Serrano, L. & Herrmann, C. A detailed thermodynamic analysis of ras/effector complex interfaces. *J. Mol. Biol.* **340**, 1039–1058 (2004).
13. Hamad, N.M. *et al.* Distinct requirements for Ras oncogenesis in human versus mouse cells. *Genes Dev.* **16**, 2045–2057 (2002).
14. Karnoub, A.E. & Weinberg, R.A. Ras oncogenes: split personalities. *Nat. Rev. Mol. Cell Biol.* **9**, 517–531 (2008).
15. Zand, T.P., Reiner, D.J. & Der, C.J. Ras effector switching promotes divergent cell fates in *C. elegans* vulval patterning. *Dev. Cell* **20**, 84–96 (2011).
16. Yeh, J.J. & Der, C.J. Targeting signal transduction in pancreatic cancer treatment. *Expert Opin. Ther. Targets* **11**, 673–694 (2007).
17. Scheffler, J.E. *et al.* Characterization of a 78-residue fragment of c-Raf-1 that comprises a minimal binding domain for the interaction with Ras-GTP. *J. Biol. Chem.* **269**, 22340–22346 (1994).
18. Warne, P.H., Viciana, P.R. & Downward, J. Direct interaction of Ras and the amino-terminal region of Raf-1 *in vitro*. *Nature* **364**, 352–355 (1993).
19. Zhang, X.F. *et al.* Normal and oncogenic p21ras proteins bind to the amino-terminal regulatory domain of c-Raf-1. *Nature* **364**, 308–313 (1993).
20. Smith, M.J., Neel, B.G. & Ikura, M. NMR-based functional profiling of RASopathies and oncogenic RAS mutations. *Proc. Natl. Acad. Sci. USA* **110**, 4574–4579 (2013).

21. Geyer, M. *et al.* Conformational transitions in p21ras and in its complexes with the effector protein Raf-RBD and the GTPase activating protein GAP. *Biochemistry* **35**, 10308–10320 (1996).
22. Spoerner, M., Herrmann, C., Vetter, I.R., Kalbitzer, H.R. & Wittinghofer, A. Dynamic properties of the Ras switch I region and its importance for binding to effectors. *Proc. Natl. Acad. Sci. USA* **98**, 4944–4949 (2001).
23. Spoerner, M., Wittinghofer, A. & Kalbitzer, H.R. Perturbation of the conformational equilibria in Ras by selective mutations as studied by 31P NMR spectroscopy. *FEBS Lett.* **578**, 305–310 (2004).
24. González-García, A. *et al.* RalGDS is required for tumor formation in a model of skin carcinogenesis. *Cancer Cell* **7**, 219–226 (2005).
25. Mishra, P.J. *et al.* Dissection of RAS downstream pathways in melanomagenesis: a role for Ral in transformation. *Oncogene* **29**, 2449–2456 (2010).
26. Vigil, D. *et al.* Aberrant overexpression of the Rgl2 Ral small GTPase-specific guanine nucleotide exchange factor promotes pancreatic cancer growth through Ral-dependent and Ral-independent mechanisms. *J. Biol. Chem.* **285**, 34729–34740 (2010).
27. Bauer, B. *et al.* Effector recognition by the small GTP-binding proteins Ras and Ral. *J. Biol. Chem.* **274**, 17763–17770 (1999).
28. Sydor, J.R., Engelhard, M., Wittinghofer, A., Goody, R.S. & Herrmann, C. Transient kinetic studies on the interaction of Ras and the Ras-binding domain of c-Raf-1 reveal rapid equilibration of the complex. *Biochemistry* **37**, 14292–14299 (1998).
29. Linnemann, T., Kiel, C., Herter, P. & Herrmann, C. The activation of RalGDS can be achieved independently of its Ras binding domain. Implications of an activation mechanism in Ras effector specificity and signal distribution. *J. Biol. Chem.* **277**, 7831–7837 (2002).
30. Herrmann, C. Ras-effector interactions: after one decade. *Curr. Opin. Struct. Biol.* **13**, 122–129 (2003).
31. Gideon, P. *et al.* Mutational and kinetic analyses of the GTPase-activating protein (GAP)-p21 interaction: the C-terminal domain of GAP is not sufficient for full activity. *Mol. Cell. Biol.* **12**, 2050–2056 (1992).
32. Eccleston, J.F., Moore, K.J., Morgan, L., Skinner, R.H. & Lowe, P.N. Kinetics of interaction between normal and proline 12 Ras and the GTPase-activating proteins, p120-GAP and neurofibromin. The significance of the intrinsic GTPase rate in determining the transforming ability of ras. *J. Biol. Chem.* **268**, 27012–27019 (1993).
33. Weber, C.K. *et al.* Mitogenic signaling of Ras is regulated by differential interaction with Raf isozymes. *Oncogene* **19**, 169–176 (2000).
34. Gureasko, J. *et al.* Membrane-dependent signal integration by the Ras activator Son of sevenless. *Nat. Struct. Mol. Biol.* **15**, 452–461 (2008).
35. Sondermann, H. *et al.* Structural analysis of autoinhibition in the Ras activator Son of sevenless. *Cell* **119**, 393–405 (2004).
36. Takashima, A. & Faller, D.V. Targeting the RAS oncogene. *Expert Opin. Ther. Targets* **17**, 507–531 (2013).
37. Hofmann, I. *et al.* K-RAS mutant pancreatic tumors show higher sensitivity to MEK than to PI3K inhibition *in vivo*. *PLoS ONE* **7**, e44146 (2012).
38. Roberts, P.J. *et al.* Combined PI3K/mTOR and MEK inhibition provides broad antitumor activity in faithful murine cancer models. *Clin. Cancer Res.* **18**, 5290–5303 (2012).
39. Kiel, C., Selzer, T., Shaul, Y., Schreiber, G. & Herrmann, C. Electrostatically optimized Ras-binding Ral guanine dissociation stimulator mutants increase the rate of association by stabilizing the encounter complex. *Proc. Natl. Acad. Sci. USA* **101**, 9223–9228 (2004).
40. Ader, C., Spoerner, M., Kalbitzer, H.R. & Brunner, E. Solid-state 31P NMR spectroscopy of precipitated guanine nucleotide-binding protein Ras in complexes with its effector molecules Raf kinase and RalGDS. *J. Phys. Chem. B* **111**, 2752–2757 (2007).
41. Spoerner, M. *et al.* Conformational states of human rat sarcoma (Ras) protein complexed with its natural ligand GTP and their role for effector interaction and GTP hydrolysis. *J. Biol. Chem.* **285**, 39768–39778 (2010).
42. Jura, N., Scotto-Lavino, E., Sobczyk, A. & Bar-Sagi, D. Differential modification of Ras proteins by ubiquitination. *Mol. Cell* **21**, 679–687 (2006).
43. Harding, A., Tian, T., Westbury, E., Frische, E. & Hancock, J.F. Subcellular localization determines MAP kinase signal output. *Curr. Biol.* **15**, 869–873 (2005).
44. Tian, T. *et al.* Plasma membrane nanoswitches generate high-fidelity Ras signal transduction. *Nat. Cell Biol.* **9**, 905–914 (2007).
45. Bivona, T.G. *et al.* PKC regulates a farnesyl-electrostatic switch on K-Ras that promotes its association with Bcl-XL on mitochondria and induces apoptosis. *Mol. Cell* **21**, 481–493 (2006).
46. Dougherty, M.K. *et al.* Regulation of Raf-1 by direct feedback phosphorylation. *Mol. Cell* **17**, 215–224 (2005).
47. Douville, E. & Downward, J. EGF induced SOS phosphorylation in PC12 cells involves P90 RSK-2. *Oncogene* **15**, 373–383 (1997).
48. Boykevisch, S. *et al.* Regulation of ras signaling dynamics by Sos-mediated positive feedback. *Curr. Biol.* **16**, 2173–2179 (2006).
49. Freedman, T.S. *et al.* A Ras-induced conformational switch in the Ras activator Son of sevenless. *Proc. Natl. Acad. Sci. USA* **103**, 16692–16697 (2006).
50. Huang, H. *et al.* Oncogenic K-Ras requires activation for enhanced activity. *Oncogene* doi:10.1038/onc.2012.619 (2013).

Acknowledgments

We thank B. Neel, G. Findlay, C. Marshall and M. Mazhab-Jafari for valuable discussion and thoughts on the manuscript. This work was supported by a grant from the Cancer Research Society (to M.I.) and in part by the Canadian Cancer Society (to M.I.) and by the Princess Margaret Hospital Foundation. M.J.S. is the recipient of a Canadian Breast Cancer Foundation Fellowship and an Ontario Cancer Institute Knudson Postdoctoral Fellowship. M.I. holds a Canada Research Chair. The Canada Foundation for Innovation funded the 800- and 600-MHz NMR spectrometers.

Author contributions

This project was conceived and designed by M.J.S. and M.I. All of the experimental work was performed by M.J.S. The manuscript was prepared by M.J.S. and M.I.

Competing financial interests

The authors declare no competing financial interests.

Additional information

Supplementary information is available in the online version of the paper. Reprints and permissions information is available online at http://www.nature.com/reprints/index.html. Correspondence and requests for materials should be addressed to M.I.

ONLINE METHODS

Plasmid constructs and antibodies. Human cDNA encoding wild-type H-RAS (Gene ID: 3265, residues 1–171) or the oncogenic mutant G12V were cloned into pET15b (Novagen/EMD Biosciences) for bacterial expression with an N-terminal His tag. The GAP-334 region from human p120GAP (Gene ID: 5921, residues 715–1047) was also subcloned and expressed in pET15b. Constructs expressing individual RBD/RA domains with N-terminal glutathione S-transferase (GST) tags were subcloned from human cDNAs into pGEX-4T2 (Amersham Pharmacia Biotech). These included: ARAF (Gene ID: 369, residues 17–94), BRAF (Gene ID: 673, residues 150–233), GRB10 (Gene ID: 2887, residues 106–351), RALGDS (Gene ID: 5900, residues 741–833), RASSF5 (Gene ID: 83593, residues 199–367), RGL1 (Gene ID: 23179, residues 681–773), RGS14-1 (Gene ID: 10636, residues 300–375) and RIN1 (Gene ID: 9610, residues 622–745). Additionally, two RAS effector domains were cloned from mouse cDNAs: AF6-1 (Gene ID: 17356, residues 37–136, which are identical to human) and Plcε1-2 (Gene ID: 74055, residues 2113–2221). We incorporated four cysteine-to-serine mutations in the GRB10 RA/PH domain to prevent aggregation, as per the previously determined crystal structure (C145S, C212S, C232S and C331S)[51]. To quantify RALA activation, human cDNA encoding the RALBP1 RAL binding domain (Gene ID: 10928, residues 395–517) was cloned and expressed in pGEX-4T2. For mammalian expression of full-length wild-type RAS and RAS^{G12V}, cDNA were subcloned into the pEGFP-C1 (Clontech) backbone, with an N-terminal Cerulean tag fused in place of EGFP. Full-length p120GAP and SOS1 (Gene ID: 6654) cDNAs were cloned and expressed from the pcDNA5/FRT/TO plasmid as part of the Flp-In T-Rex system (Invitrogen) for generating stable, Tet-inducible expression lines. CaaX-tagged SOS^{cat} (residues 565–1064) and the activated SOS1 DH/Link mutant (incorporating mutations E268A, M269A, D271A and R552G) were also generated in the pcDNA5/FRT/TO plasmid. All of the constructs were sequence verified.

The anti-Flag M2 (cat. no. F3165; 1:1,000) and anti-tubulin (cat. no. T9026; 1:1,000) mAbs were purchased from Sigma, and anti-RALA (cat. no. 610221; 1:2,500) from BD Biosciences (Transduction Labs). Rabbit polyclonal anti-ERK (cat. no. 06-182; 1:1,000) and anti-RAS (cat. no. 05-1072; 1:1,000) antibodies were from Millipore, anti-pERK (cat. no. 9101S; 1:1,000) was from Cell Signaling Technology, and anti-GFP (cat. no. ab290; 1:5,000) was from Abcam.

Purification of recombinant proteins. GST- or His-tagged proteins were expressed in *E. coli* BL21 cells grown in minimal or LB medium by induction with isopropyl-β-D-thiogalactopyranoside (IPTG) at 15 °C overnight. Generally, cells were lysed and sonicated in 20 mM Tris (pH 7.5), 150 mM NaCl, 10% glycerol, 0.4% NP-40, protease inhibitors (Roche), 1 mM phenylmethylsulfonyl fluoride (PMSF), 10 ng ml^{-1} DNase and either 1 mM dithiothreitol or 10 mM β-mercaptoethanol. Lysate was cleared by centrifugation and incubated with glutathione (Amersham Pharmacia Biotech) or Ni-NTA (Qiagen) resin at 4 °C for 2 h. Bound proteins were eluted directly with thrombin cleavage or with 250 mM imidazole (Bioshop) followed by thrombin. Concentrated proteins were purified to homogeneity by size-exclusion chromatography using either an S75 or S200 column (GE Healthcare). Recombinant wild-type RAS is purified from *E. coli* predominantly in the GDP-bound form, whereas G12V is regularly bound to GTP. These proteins were preloaded with GMPPNP, GTP, GTPγS or GDP (Sigma) when required.

Cell culture. HEK 293T cells were maintained in Dulbecco's Modified Eagle's Medium containing 10% FCS and antibiotics. For exogenous expression, cells were transiently transfected with PEI[52]. Full-length p120GAP stable cell lines were derived using the Flp-In T-Rex protocol (Invitrogen). Tet-induction was done with 2 μg ml^{-1} over 48 h. EGF (PeproTech Inc.) was added after culturing overnight in the absence of serum. For NMR assays, transfected cells were lysed in NMR buffer (20 mM Tris (pH 7.5), 100 mM NaCl, 1 mM DTT and 5 mM $MgCl_2$) plus detergent (1% Triton X-100) and protease inhibitors. These lysates were cleared by centrifugation.

NMR spectroscopy. All NMR data were recorded at 25 °C on an 800-MHz Bruker AVANCE II spectrometer equipped with a 5-mm TCI CryoProbe or 600-MHz Bruker UltraShield spectrometer with a 1.7-mm CryoProbe. NMR samples were prepared in buffer containing 20 mM Tris (pH 7.5), 100 mM NaCl, 1 mM DTT, 5 mM MgCl2 and 10% D2O unless otherwise noted. Spectra were processed with NMRPipe[53] and analyzed using NMRView[54].

NMR-based GTPase assay and effector mixing. For GTPase analysis, RAS concentration was held consistent at 250 μM. To calculate the GDP/GTP-bound ratio (I_{GDP} / (I_{GDP} + I_{GTP})), peak intensities were extracted from individual spectrum with NMRView on at least eight paired resonances, they were plotted against time, and data were fit to a one-phase exponential or sigmoidal curve using GraphPad Prism. GAP assays in the presence of effector binding domains were plotted using only GDP intensities, as many GTP-specific resonances undergo large chemical shift perturbations upon effector binding. Resulting hydrolysis rates were identical to those calculated using the (I_{GDP}/(I_{GDP} + I_{GTP})) ratio, providing the reaction reached completion. All of the exchange assays were performed in a tenfold molar excess of GTPγS to preclude competition with hydrolysis. For effector RBD mixing, RAS proteins were preloaded with GMPPNP and used at 100 μM. Effector domain concentrations were steady at twofold molar excess to RAS (200 μM) and were mixed simultaneously for competition studies, followed by a 30-min equilibration period at 25 °C. Peak intensities at chemical shift coordinates characteristic of specific RBD interactions were extracted with NMRView for at least five well-dispersed resonances in each pairwise competition.

ITC. RAS interactions with effector domains were measured using a Microcal VP-ITC instrument. Stock solutions were diluted into filtered and degassed 20 mM Tris (pH 7.5), 100 mM NaCl, 5 mM $MgCl_2$ and 1 mM DTT. Experiments with the ARAF-RBD were carried out at 30 °C and with RGL1-RA at 25 °C. Heats of dilution were determined from control experiments in which RAS binding domains were titrated into buffer alone plus 500 μM GMPPNP. Data were fitted using the software Origin 7 (Microcal).

Cell-based analysis of effector signaling. Transfected cells were lysed in TXNP buffer (20 mM Tris (pH 7.5), 150 mM NaCl, 10% glycerol, 1% Triton X-100, 1% NP-40, 1 mM DTT, 5 mM $MgCl_2$, 1 mM sodium vanadate, 1 mM PMSF and protease inhibitors), and lysates were cleared by centrifugation. A fraction of each lysate were separated by SDS-PAGE and transferred to a nitrocellulose membrane (Schleicher and Schuell Bioscience). Remaining lysates were used for determining RALA-GTP levels, performed immediately with glutathione beads carrying recombinant GST-tagged RALBP1-RBD. Equal amounts of beads were added to lysates and incubated for 15 min at 4 °C, followed by washing four times with TXNP buffer, separation by SDS-PAGE and transfer to a nitrocellulose membrane. Membranes were blocked in TBST containing 5% skim milk and immunoblotted. Primary antibodies were detected with anti-mouse Ig (Bio-Rad; cat. no. 170-6516; 1:10,000) or anti-rabbit Ig (Bio-Rad; cat. no. 170-6515; 1:10,000) antibodies conjugated to horseradish peroxidase followed by treatment with ECL (Pierce). Densitometry quantifications of pERK and RALA were done using ImageJ.

Statistical analysis. For direct comparison of two data sets, two-tailed *t*-tests (unpaired or paired, $P < 0.05$ or $P < 0.01$) were used. For fit of averaged hierarchical data, we used $Y = Y_{max} \times (1 - \exp(-K \times X))$ or $Y = \text{start} \times \exp(K \times X)$ and added the constraints that 0% RBD binds 0% RAS or that 100% RBD binds 100% RAS.

51. Depetris, R.S., Wu, J. & Hubbard, S.R. Structural and functional studies of the Ras-associating and pleckstrin-homology domains of Grb10 and Grb14. *Nat. Struct. Mol. Biol.* **16**, 833–839 (2009).
52. Boussif, O. *et al.* A versatile vector for gene and oligonucleotide transfer into cells in culture and *in vivo*: polyethylenimine. *Proc. Natl. Acad. Sci. USA* **92**, 7297–7301 (1995).
53. Delaglio, F. *et al.* NMRPipe: a multidimensional spectral processing system based on UNIX pipes. *J. Biomol. NMR* **6**, 277–293 (1995).
54. Johnson, B.A. Using NMRView to visualize and analyze the NMR spectra of macromolecules. *Methods Mol. Biol.* **278**, 313–352 (2004).